

Research Paper

NIR-Cyanine Dye Linker: a Promising Candidate for Isochronic Fluorescence Imaging in Molecular Cancer Diagnostics and Therapy Monitoring

Dorde Komljenovic¹✉, Manfred Wiessler¹, Waldemar Waldeck², Volker Ehemann³, Ruediger Pipkorn⁴, Hans-Hermann Schrenk¹, Jürgen Debus⁵, and Klaus Braun¹#

1. German Cancer Research Center, Department of Medical Physics in Radiology, INF 280, 69120 Heidelberg, Germany
2. German Cancer Research Center, Division of Biophysics of Macromolecules, INF 580, 69120 Heidelberg, Germany
3. University of Heidelberg, Institute of Pathology, INF 224, 69120 Heidelberg, Germany
4. German Cancer Research Center, Department of Translational Immunology, INF 580, 69120 Heidelberg, Germany
5. University of Heidelberg, Department of Radiation Oncology, INF 400, 69120 Heidelberg, Germany

#deceased

✉ Corresponding author: Dr. Dorde Komljenovic. E-mail: d.komljenovic@dkfz.de. Phone number: +49(0)6221422686

© Ivyspring International Publisher. Reproduction is permitted for personal, noncommercial use, provided that the article is in whole, unmodified, and properly cited. See <http://ivyspring.com/terms> for terms and conditions.

Received: 2014.12.30; Accepted: 2015.08.07; Published: 2016.01.01

Abstract

Personalized anti-cancer medicine is boosted by the recent development of molecular diagnostics and molecularly targeted drugs requiring rapid and efficient ligation routes. Here, we present a novel approach to synthesize a conjugate able to act simultaneously as an imaging and as a chemotherapeutic agent by coupling functional peptides employing *solid phase peptide synthesis* technologies. Development and the first synthesis of a fluorescent dye with similarity in the polymethine part of the Cy7 molecule whose indolenine-N residues were substituted with a propylene linker are described. Methylating agent temozolomide is functionalized with a tetrazine as a diene component whereas Cy7-cell penetrating peptide conjugate acts as a dienophilic reaction partner for the inverse Diels-Alder click chemistry-mediated ligation route yielding a theranostic conjugate, 3-mercapto-propionic-cyclohexenyl-Cy7-bis-temozolomide-bromide-cell penetrating peptide. Synthesis route described here may facilitate targeted delivery of the therapeutic compound to achieve sufficient local concentrations at the target site or tissue. Its versatility allows a choice of adequate imaging tags applicable in e.g. PET, SPECT, CT, near-infrared imaging, and therapeutic substances including cytotoxic agents. Imaging tags and therapeutics may be simultaneously bound to the conjugate applying *click chemistry*. Theranostic compound presented here offers a solid basis for a further improvement of cancer management in a precise, patient-specific manner.

Key words: Click chemistry; inverse Diels-Alder reaction; fluorescent dye; molecular diagnostics; multimodal imaging; near infrared imaging; solid phase peptide synthesis.

Introduction

The success in extent and sustainability of therapeutic interventions against cancer primarily depends on the quality and precision of the diagnostic technologies. The interaction of newly synthesized ligands with aberrantly expressed receptors as target proteins, can fulfil requirements for molecular diagnostics by the use of molecular imaging (MI) and for

therapeutic regimens for individualized patient-specific treatment (targeted therapy).

The identification of specific amino acid sequences as structures of target proteins and the ensuing development of such ligand molecules require very exigent chemical ligation methods. We combined the well-established Diels-Alder reaction (DAR) [1,2]

and the DAR with inversed electron demand (DAR_{inv}) with the *solid phase peptide synthesis* (SPPS) [3-5]. These techniques are considered as critical pillars for re-formulation of classical drugs.

Technically, the functionalization of nucleic acids and their derivatives with thiol-groups for oxidative connection of functional peptides was documented [6]. The synthesis of disulfide- functionalized molecules was also described [7-10].

Our approach relies on the coupling of SH-groups to fluorescent dyes via a 3-mercapto-propionic acid linker using a *cell penetrating peptide* (CPP) for membrane transport. By the use of SPPS we synthesized the reaction product 3-mercapto-propionic-cyclohexenyl-Cy7-bis-norborne nyl-bromide-CPP conjugate. This methodology may be used to assess not only morphological structures but also metabolic processes within tissues or cells employing positron emission tomography (PET), magnetic resonance imaging (MRI) and single photon emission computed tomography (SPECT) [11].

The use of fluorescent dyes deriving from *cyanine polymethine* (Cy) family (Cy3 - Cy7) for biomedical imaging is well-documented [12-16]. These fluorochromes reveal a broad variability in chemical stability.

Here, we describe the development and the first synthesis of a fluorescent dye with similarity in the polymethine part of the Cy7 molecule whose indole-*N* residues were substituted with a propylene linker. This linker can be functionalized with norbornene, and/or alkyne groups. These functional molecules are not only restricted to a function as a linker. They also act as a dye in near infrared (NIR) imaging and, as an additional feature; they can be functionalized as a bi-functional linkers. The variability of conjugated SH-groups of the different Cy-based dyes facilitates the use of a broad spectrum of FI molecules. Such linkers may in particular be applicable for the development of agents used in MI employing NIR fluorescence methods [17-21] during patient-specific treatment under non-invasive conditions.

As a therapeutic modality, here we functionalized a Cy7-like dye initially with {8-carbamoyl-3-(2-chloroethyl)imidazo[5,1-*d*]-1,2,3,5-tetrazine-4(3*H*)-one} temozolomide (TMZ) acting as a methylating agent [22]. We functionalized TMZ using a ligation procedure described previously [23]. The effects on the phenotypical change of different primary glioblastoma cells were reported by the Wiessler group [24]. The prototype theranostic conjugate described here acting as both a contrast agent (CA) and as a multi-faceted therapeutic molecule, functionalized with old fashioned anti-cancer drugs can improve

effectiveness of anti-cancer interventions and enable monitoring of cellular phenotype change and cell killing effects caused by local enrichment of a cytotoxic agent [14].

Material and methods

Biological Methods

Cell culture

We used Dunning rat prostate tumor subline R3327 (kind gift from J. Langowski, Department of Biophysics of Macromolecules, German Cancer Research Center, Heidelberg, Germany), metastatic rat prostate tumor cells MAT_{Ly/Lu} (ATCC® CRL-2376™), human prostate cancer cells DU-145 (ATCC® HTB-81™) as well as metastatic breast cancer cells MDA-MB-231 (ATCC® HTB-26™). R3327, DU-145, MDA-MB-231 and MAT_{Ly/Lu} cells were maintained at 37°C in a 5% CO₂ atmosphere in RPMI 1640 Medium (GlutaMAX™ Supplement, 61870, Gibco®, Germany) and RPMI 1640 Medium (ATCC modification, A10491, Invitrogen), respectively.

Cell contamination test and authentication report

To avoid the issues of cross-contamination and misidentification of cell lines, standardized *multiplex cell contamination test* (Multiplexion, Germany, purchase No.: 45369600) and *cell line authentication test* (MCA) (Multiplexion, Germany, purchase No.: 45376089) were conducted confirming the absence of contaminations and the authentication of examined cell lines.

Treatment of carcinoma cell lines

R3327 cells (5×10^5) were treated in sterile, four compartments CELLview™ Cell Culture Dishes 35 × 10 mm, with advanced TC™ surface (627975, Greiner Bio-One, Germany) in cell culture medium with a dilution of the 3-mercapto-propionic-cyclohexenyl-Cy7-bis-TMZ-bromide-CPP conjugate **12** (final concentration 100 μM) which was dissolved as stock solution in 50% acetonitrile/H₂O_{bidest.} Cells were grown as sub-confluent monolayer in the RPMI (control) and the effects were analyzed 20 min, 24 h and 48 h after the onset of treatment.

All studies with the subline R3327-MAT_{Ly/Lu} and with the DU145 and MDA-MB-231 cell lines occurred under identical treatment conditions (*supplementary information* [Figure S7]).

Functionality studies by confocal laser scanning microscopy (CLSM)

We used a Leica confocal microscope TCS SP5 II (objective 63-fold) and examined the images with Leica LAS-AV software. Investigated cells were

stained using the wheat germ agglutinin (WGA) Alexa Fluor® 488 conjugate (4 µg/ml, W11261, Life Technologies GmbH, Germany) according to the manufacturer's instructions. The following laser power was used for Cy7, DAPI and WGA Alexa Fluor® 488 conjugate: 643-800 nm, 415-466 nm and 498-547 nm, respectively.

Cell cycle analysis

High resolution flow cytometric analyses were performed using a PAS II flow cytometer (Partec, Munster/Germany) equipped with a mercury lamp 100W and filter combination for DAPI stained single cells. Natively sampled cells were isolated with 2.1% citric acid/0.5% Tween®20 according to the method for high resolution DNA and cell cycle analyses at the room temperature under mild shaking. Phosphate buffer (7.2 g Na₂HPO₄ × 2H₂O in 100 ml distilled H₂O) pH 8.0 containing DAPI was used [25]. Each histogram represents DNA-index and cell cycle for 20000 cells. For histogram analyses we used the Multicycle software (Phoenix Flow Systems, San Diego, CA).

Multiparametric flow cytometry analysis

Multiparametric analysis was done using a Galaxy pro flow cytometer (PARTEC, Münster, Germany) by stimulating the fluorochromes DAPI with a mercury 100 W vapour lamp, FITC with a 488 nm air cooled argon laser and measuring the fluorescence intensities at 530/30 nm, and Cy7 with an red laser diode excitation 635 nm and emission at 780/60 nm. Green and red fluorescence were measured in a logarithmic whereas DAPI stained DNA in linear mode. For each measurement 20000 cells were used. Multiparametric acquisition and analyses were obtained using the Flowmax software (PARTEC, Münster, Germany).

Chemical Procedures

Synthesis of the Cy7-like fluorescent dye building blocks

The schemes describe the steps of the synthetic ways from the educts via intermediates to the different 3-mercapto-propionic-cyclohexenyl-Cy7-based monomer products: the symmetrical **12** (bis-norbornenyl-) variant. Molecule numbers and compound names: *supplementary information* [Figure S1]. Corresponding reaction schemes and chromatograms are listed in *supplementary information*.

Synthesis of the norbornenyl-aminopropyl-indolenium-bromide (**5**)

The synthesis of the norbornene-5-exo-carboxylic acid chloride **4** was carried out according to the synthesis protocol published by

Boehme et al [26]. The synthesis of aminopropyl-indolenium-bromide **3** was published by the Maiti group [27]. The residues **3** and **5** were purified by preparative HPLC on a Kromasil 100-C18-10 µm reverse phase column (30 × 250 mm) using an eluent of 0.1% trifluoroacetic acid in water (A) and 80% acetonitrile in water (B). The product was eluted with a linear gradient of 10% B to 80% B in 30 min at a flow rate of 23 ml/min. The calculated mass [m/e] of **3**: 217.17 (100.0%); molecular formula C₁₄H₂₁N₂. Corresponding reaction scheme: *supplementary information* [Figure S2].

Synthesis of the chloro-cyclohexenyl-Cy7-bis-norbornenyl-bromide (**7**)

Synthesis and characterization of heptamine cyanine dyes are well described by the Li group [28]. The calculated mass [m/e]: m/e: 337.23 (100.0%); molecular formula C₂₂H₂₉N₂O⁺. Corresponding reaction schemes and chromatograms: *supplementary information* [Figure S3]. The synthesis of the product **7** was carried out according the synthesis protocol published by Li and by Reynolds and Drexhage [29]. The product 2-chloro-1-formyl-3-(hydroxymethylene)-1-cyclohexene **6** was purified by preparative HPLC on a Kromasil 100-C18-10 µm reverse phase column (30 × 250 mm) as described above. The measured mass [m/e]: 809.4; the calculated mass [m/e]: 809.46 (100.0%); chemical formula: C₅₂H₆₂ClN₄O₂⁺. Corresponding reaction scheme, chromatogram and TOF MS ES⁺ spectrometry diagram: *supplementary information* [Figure S3].

Synthesis of the 3-mercapto-propionic-cyclohexenyl-Cy7-bis-norbornenyl-bromide building block (**9**)

The principle of the synthesis of **9** was documented by the Hilderbrand group in 2005 [30].

The product **9** was purified using HPLC as described above. Calculated mass [m/e]: 879.49 (100.0%); chemical formula: C₅₅H₆₇N₄O₄S⁺; the resulting yield: 150 mg = 13%. Corresponding reaction schemes and chromatogram: *supplementary information* [Figure S4].

Reformulation of the pharmacologically active substance

Synthesis of the diaryl-tetrazine-TMZ (**10**)

The molecule **10** was used as an active component for the cell toxicity studies. The synthesis steps for the functionalization of TMZ with *N*-(2-aminopropyl)-4-(6-(pyrimidine-2-yl)-1,2,4,5-tetrazine-3-yl)benzamide are documented [24,31-33]. Exact mass: 513.2 [m/e]; molecular weight: 513.5; (100.0%). Chemical formula: C₂₂H₁₉N₁₃O₃; measured mass: 536.3 (+Na) [m/e]; yield: 87%. Corresponding structural

formula, chromatogram and spectra: *supplementary information* [Figure S5].

SPPS of the 3-mercapto-propionic-cyclohexenyl-Cy7-bis-norbornenyl-bromide-CPP (11)

We synthesized the 3-mercapto-propionic-cyclohexenyl-Cy7-bis-norbornenyl-bromide-CPP-conjugate with the amino acid sequence CRQIKIWFQNRRMKWKK (CPP) facilitating the passage across cell membrane in an automated multiple synthesizer Syro II (MultiSyn Tech, Germany) using the Fmoc chemistry under atmospheric conditions at room temperature as follows: 0.25 μmol of Fmoc-L-Arg(Pbf)-HMPB-ChemMatrix® resin loading 0.50 mmol/g.

The product **11** was achieved with a fivefold excess of the Fmoc-protected amino acid and was activated in situ with 5 equivalents 2-(1H-benzotriazole-1-yl)-1,1,3,3-tetramethyluronium hexafluorophosphate (HBTU) and *N,N*-diisopropylethylamine (DIPEA) (0.5 M) in *N,N*-dimethylformamide (DMF). In a final step, the 3-mercapto-propionic-cyclohexenyl-Cy7-bis-norbornenyl-bromide **9** was coupled. The reaction time was 40 min. After each step the resin was washed 5 times with DMF and after completion the resin was washed three times with dichloromethane (DCM) and iso-propanol and dried.

The following cleavage of the peptide **11** from the resin and of the side chain protecting groups was performed for 4 h at room temperature with trifluoroacetic acid (TFA) (95%) and triethylsilane (TIS)/water (2.5%/2.5%) as scavenger in water. The calculated mass: 3108.73 [m/e]: 3110.74 (100.0%), chemical formula: $\text{C}_{159}\text{H}_{231}\text{N}_{36}\text{O}_{25}\text{S}_2^+$; yield: 10 mg (20.5%). Corresponding structural formula, chromatogram and spectra: *supplementary information* [Figure S6].

Click chemistry-mediated ligation reactions used for the synthesis of the final theranostic conjugate

Synthesis of the 3-mercapto-propionic-cyclohexenyl-Cy7-bis-TMZ-bromide-CPP (12)

Before ligation of the pharmacologically active 4-methyl-5-oxo-2,3,4,6,8-pentazabicyclo[4.3.0]nona-2,7,9-triene-9-carboxamide (temozolomide (TMZ), Sigma-Aldrich, Germany) the functionalization of TMZ with *N*-(2-aminopropyl)-4-(6-(pyrimidine-2-yl)-1,2,4,5-tetrazine-3-yl)benzamide (**10**) as a diene component was required [14,24,31]. **10** acts as a diene partner and the 3-mercapto-propionic-cyclohexenyl-Cy7-bis-norbornenyl-bromide-CPP **11** as a dienophilic reaction partner for the DAR_{inv} click chemistry-mediated ligation. The resulting DAR_{inv} product **12** offers the mandatory properties of a theranostic

agent.

Purification of the conjugates

Purification of the end product conjugate **12** (Figure 1) was performed by semi-preparative reversed-phase HPLC (Dionex (Idstein, Germany): Ultimate 3000 LPG-3400A pump and variable four wavelength Ultimate 3000 VWD-3400RS UV/VIS detector (222 nm, 254 nm, 280 nm); column: Chromolith Performance RP-18e column (100 \times 10 mm; Merck, Darmstadt, Germany). The solvent gradient was raised from 5% to 100% acetonitrile in 5 min at a flow rate of 6 ml/min. The aqueous phase consisted of water containing 0.1% TFA. $t_{\text{R}} = 3.58$ min. The fractions containing the purified peptide were lyophilized. The purified material was characterized with analytical HPLC and matrix assisted laser desorption mass spectrometry. The measured mass: 4138 +5H⁺ [m/e]. The calculated mass [m/e]: 4133.11 (100.0%); chemical formula $\text{C}_{207}\text{H}_{273}\text{N}_{58}\text{O}_{31}\text{S}_2^+$.

Results

Cell localization studies of the 3-mercapto-propionic-cyclohexenyl-Cy7-bis-norbornenyl-bromide CPP conjugate **11** using CLSM

Firstly, we investigated the uptake of the 3-mercapto-propionic-cyclohexenyl-Cy7-bis-norbornenyl-bromide-CPP molecule **11** in different cell lines. To ensure the functionality of **11**, cancer cell lines DU-145 (A,B,C,D), MDA-MB-231 (E,F,G,H), MAT_{Ly/Lu} (J,K,L,M), and R3327 (N,O,P,Q) were treated with the conjugate **11** as illustrated in Figure 2. Row **1** presents images of the cancer cell lines under the laser light fluorescence conditions before treatment with **11** as an untreated control.

Images A, E, J, and N depict a control Alexa Fluor® 488-WGA (wheat germ agglutinin) staining and show green fluorescence signals close to the cell membrane after 20 min incubation. Clear blue fluorescence signals obtained using DAPI show the deoxyribonucleic acid (DNA) inside the nuclei except J (MAT_{Ly/Lu}) in which the nucleus-located blue fluorescence is hardly detectable (row **2**).

Images B, F, K, and O (row **3**) show the cell lines derived from different tumor entities and offer differentially pronounced NIR fluorescence signals (red color of the Cy7-like dye) after 20 min incubation with **11** (100 μM final concentration) in the cytoplasm and perinuclearly. The nuclear space reveals blue DAPI fluorescence. The speckle-like green fluorescence signals (Alexa Fluor® 488-WGA) are clearly visible in all investigated cell lines, except in the MDA-MB-231 cells (F), in which only a weak green fluorescence signal could be detected.

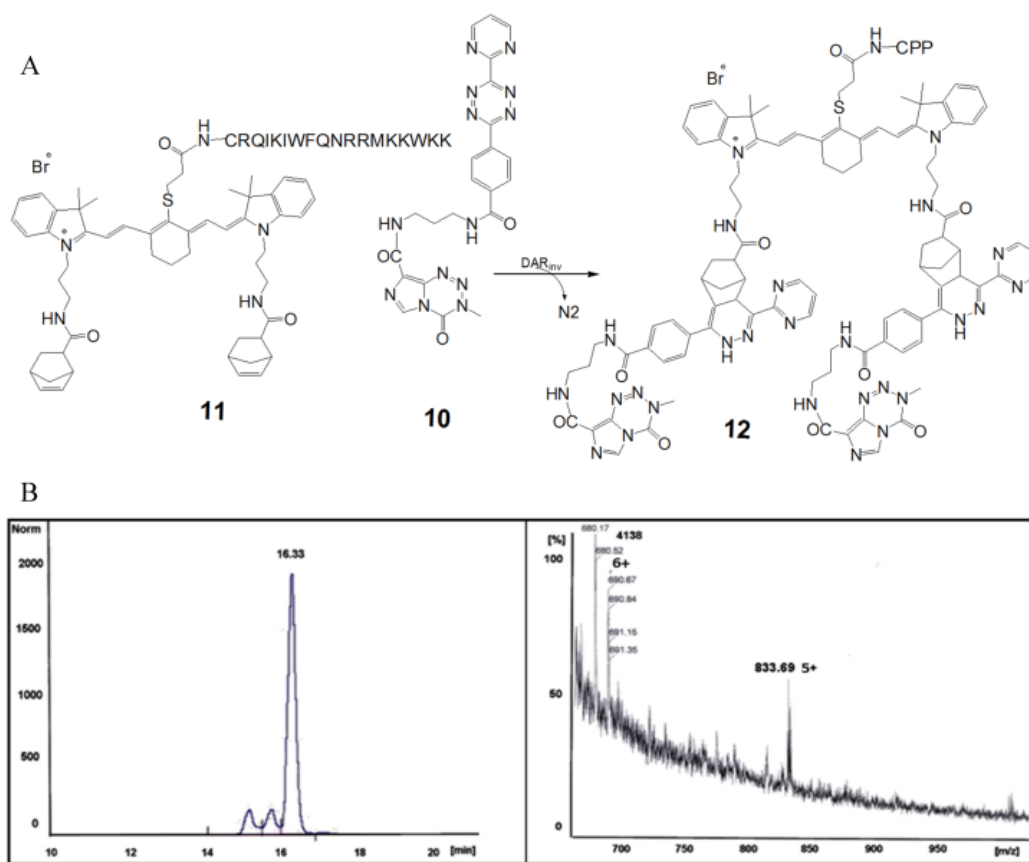


Figure 1. A. Partially schematized structural formula and the chemical reaction step of the complete 3-mercapto-propionic-cyclohexenyl-Cy7-bis-TMZ-bromide-CPP 12. This fluorescent peptide conjugate 12 mainly consists of the amino acid sequence of the CPP connected via the thioether of the 3-mercapto-propionic-cyclohexenyl-Cy7-bis-norbornenyl-bromide. The norbornenes act as dienophilic reaction partners in the DAR_{mv} . According to the protocols of Saracoglu [50] and Hansell [51] we coupled **11** with **10**. Using *click reaction* we synthesized the final reaction product **12**. **B. Quantitative analysis in HPLC and MS spectrograph of the reaction product 12.** The peak of the retention time was measured at 16.33 min. The relative amount of the peak area was 78.5%. The MS spectrograph shows the m/e 690.67/833.69 representing the sixfold/fivefold cation of the calculated isotope pattern and demonstrates the identity of the reaction product **12**.

After 24 h treatment with **11** none of the tested cell lines showed any morphological change. Each cell line clearly exhibited all tested fluorescence signals, showing the following cellular structures: nucleus (blue), cytoplasm (red) and cell membrane (green) (row **4**). In the DU-145 (C) and in the MAT_{Ly/Lu} cells (L) a slight trend to speckle formation was noticed. Of note, DU-145 (C) and R3327 (P) cells reveal a clear localization of the red fluorescence signals around the nuclei with increased signal intensity in the direction of the nuclei in DU-145 cells, whereas in R3327 cells a radial distribution around the nuclei was visible. We observed that the tested cell lines did not exhibit signs of morphologic membrane damage. It was conspicuous that the R3327 cells and its metastatic subline MAT_{Ly/Lu} showed a trend towards formation of spherical structures (L), whereas the DU-145 grew as a monolayer (C). The cell membranes regularly revealed a clear green fluorescence arising from the exposure to Alexa Fluor® 488-WGA (row **4**).

After 48h treatment with the conjugate **11** the signal intensity of red fluorescence decreased as seen in the respective images (D,H,M,Q) shown in row **5**.

This observation also applied for the blue signal intensity. The fluorescence intensity of the green fluorescence signal derived from the WGA staining of the cell membranes was increased and remained nearly unchanged, with the exception of cell membranes of the DU-145 cells, which exhibited hardly detectable green fluorescence signals. However the trend for the speckle formation continuously increased with time, a phenomenon which could be explained by aging-caused depletion processes during the length of time of the cell culture experiments. All these findings could be explained with tentative general changes of the cellular phenotype or DAPI (DNA) depletion processes during the progressing experimental time.

The aim of this step of the experiment was to monitor the cellular phenotype during the course of the experiment after treatment with intracellular fluorescent dye 3-mercapto-propionic-cyclohexenyl-Cy7-bis-norbornenyl-bromide-CPP **11** without the methylating agent TMZ. These findings are of importance for the forthcoming studies during which pharmacologically active cytotoxic molecules are used.

Analyses of the cell phenotype after treatment with 3-mercapto-propionic-cyclohexenyl-Cy7-bis-TMZ-bromide-CPP 12 using CLSM

Here, we assessed the impact of 12 on the phe-

notype of the investigated cancer cell lines (Figure 3: R3327 cells; *supplementary information* [Figures S7A, S7B, and S7C]: Mat_{Ly/Lu}, DU-145, and MDA-MD-231 cells, respectively).

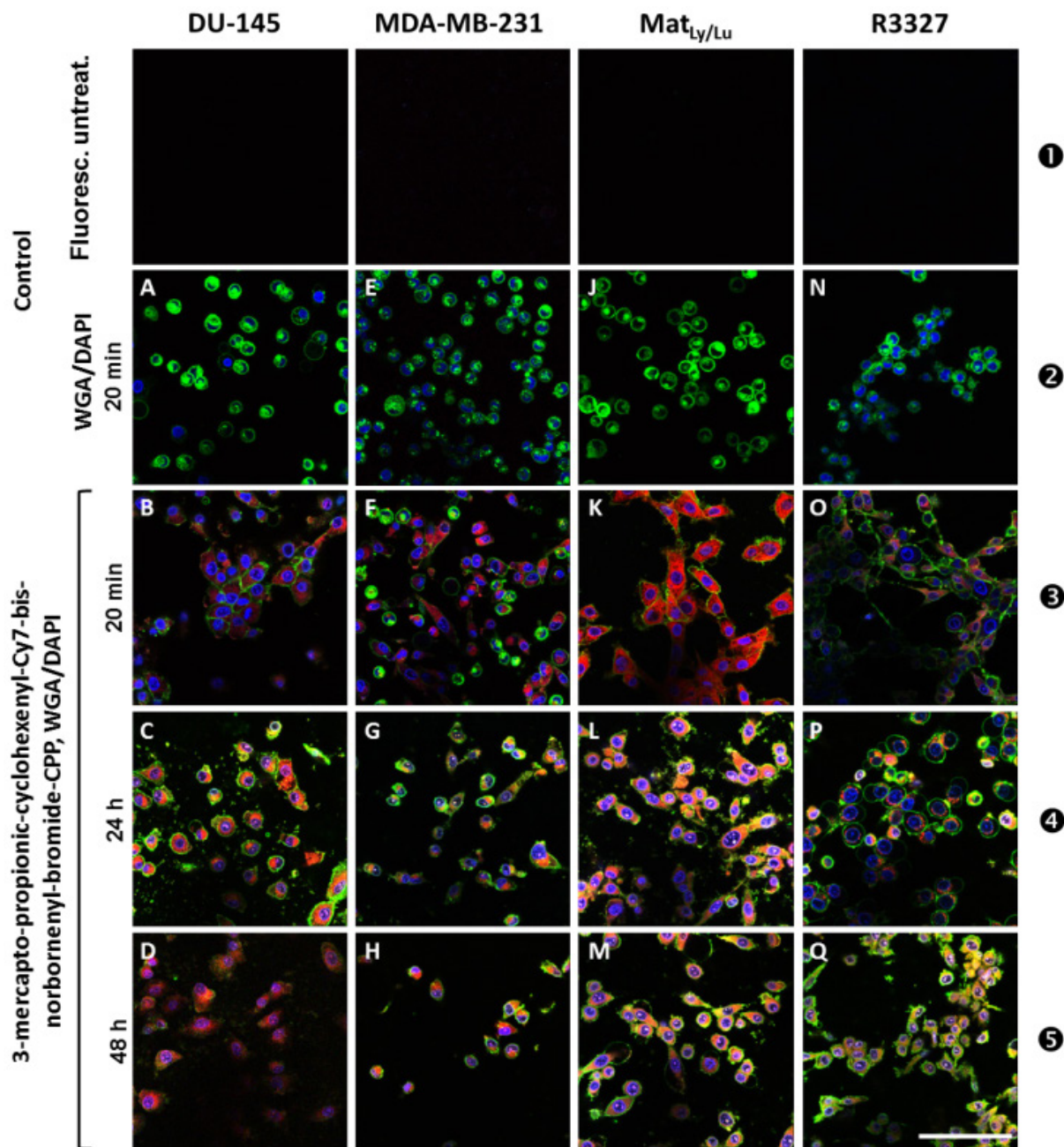


Figure 2. CLSM analyses of DU-145 (A,B,C,D), MDA-MB-231 (E,F,G,H), MAT_{Ly/Lu} (J,K,L,M), and R3327 (N,O,P,Q) cell lines. Row ❶ depicts the tested cell lines under laser light-induced fluorescence conditions but untreated; no fluorescence signal could be observed in these images. Row ❷ (images A,E,J,N) exhibits the corresponding control cells, treated with Alexa Fluor® 488-WGA and DAPI but without 11. The extensive presentation of the cell membranes was carried out by Alexa Fluor® 488-WGA (green fluorescence) and of the nuclei with DAPI staining (blue). Rows ❸ (B,F,K,O), ❹ (C,G,L,P) and ❺ (D,H,M,Q) depict investigated cell lines 20 min, 24 h and 48 h after the onset of treatment with 11 at a final concentration of 100 µM. Scale bar: 100 µm.

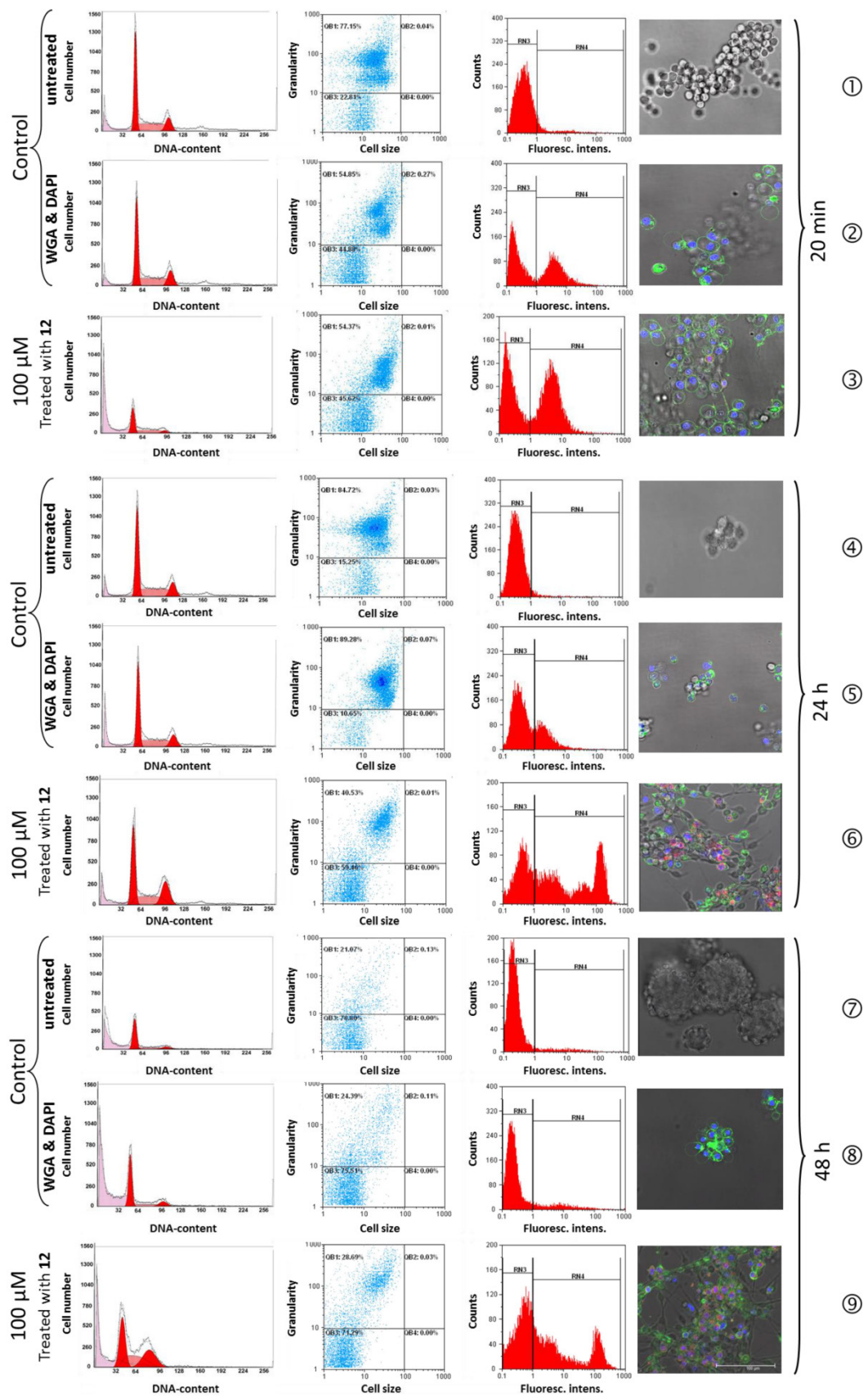


Figure 3. Effect of 12 on the cell cycle distribution (column 1), granularity/cell size ratio (column 2), cell counts/fluorescence intensity ratio (column 3) and the CLSM-assessed change of the cell phenotype (column 4) of R3327 cells. Untreated control (①,④,⑦); WGA and DAPI-stained (②,⑤,⑧) and 12-incubated, WGA and DAPI-stained (③,⑥,⑨) R3327 cells (incubation time: 20 min, 24 h, and 48 h, respectively). The changes of the phenotype and the cell cycle of the treated cells were monitored by bright-field/CLSM fluorescence (column 4). Corresponding analyses of Mat^{Low}/L^{Low} DU-145 and MDA-MB-231 cells incubated with WGA and DAPI with and without 12 under identical treatment conditions: *supplementary information* [Figures S7A, S7B and S7C, respectively]. Scale bar: 100 μm.

Table 1. Amount of the cell cycle fractions (%) of untreated and WGA/DAPI-stained control cells compared to cells treated with **12**, 0 h, 24 h, and 48 h after the onset of treatment.

A R3327												
	Control				WGA/DAPI				TMZ-Cy			
	G1	G2/M	S	Cell debris	G1	G2/M	S	Cell debris	G1	G2/M	S	Cell debris
0 h	49,5	14,7	35,80	17	46,8	16,5	36,6	12,6	49,8	9,5	40,6	57,6
24 h	49,4	15	35,4	13	49,5	14,9	35,3	23,1	43,8	26,1	29,9	15,8
48 h	67,9	11,6	20,4	49	68,4	15,3	16,1	66,4	38,1	30	31,7	32,6

B DU-145												
	Control				WGA/DAPI				TMZ-Cy			
	G1	G2/M	S	Cell debris	G1	G2/M	S	Cell debris	G1	G2/M	S	Cell debris
0 h	76	11	12,80	5,9	75,1	11,5	13,3	8	77,3	9,8	12,8	14,8
24 h	77,2	11,7	10,9	11	78,1	10,2	11,5	13,7	57,7	11,8	30,3	19,9
48 h	85,7	6,8	7,3	8,9	85,9	7,4	6,8	4,4	70,2	6,6	23	43,4

C MDA-MB-231												
	Control				WGA/DAPI				TMZ-Cy			
	G1	G2/M	S	Cell debris	G1	G2/M	S	Cell debris	G1	G2/M	S	Cell debris
0 h	71,5	11,2	17,10	10,1	70,7	11,5	17,6	12,8	71,4	11,9	16,5	17,2
24 h	64,7	9	26,1	10,6	64,3	9,1	26,5	10,9	67,4	11,4	21,1	25,2
48 h	68,2	10,3	21,4	11	67,5	11,8	20,6	5,7	65,7	8,2	26	41,5

D MAT Lv/Lu												
	Control				WGA/DAPI				TMZ-Cy			
	G1	G2/M	S	Cell debris	G1	G2/M	S	Cell debris	G1	G2/M	S	Cell debris
0 h	69,9	13,8	16,10	10,4	70,9	12,5	16,5	15,1	69,6	11,9	18,4	12,1
24 h	74,9	12,7	12,2	15	75,2	12,9	11,7	12,3	58	20,7	21,1	14
48 h	64,3	17,2	18,4	8,2	67,8	13,9	18,2	23,1	53,2	21,5	25,1	27,5

Flow cytometry cell cycle analyses of R3327 cells after treatment with 3-mercaptopropionic-cyclohexenyl-Cy7-bis-TMZ-bromide-CPP (**12**)

No morphological difference was observed between the WGA and DAPI-stained, 20 min 3-mercaptopropionic-cyclohexenyl-Cy7-bis-TMZ-bromide-CPP-treated R3327 cells and the untreated control cells. All control cells presented as morphologically unaffected at a nearly identical rate in the S-phase (35.8% and 36.6%) and in the G₂/M-phase (14.7% and 16.5%). The cell cycle analysis of cells treated with **12**, revealed 49.8% G₀/G₁-phase, similar to the G₀/G₁-fraction in the control cells (49.5% and 46.8%), but an increased amount of cells in the S-phase (40.6%) and a decreased cell number in the G₂/M-phase (9.5%) (Table 1 A).

After 24 h treatment with **12** an initial change of the cellular phenotype occurred (Figure 3, row 6). As shown in the image, cell membrane fragments could be observed indicating membrane damage processes. The cell cycle analyses of the control cells (Figure 3, rows 4 and 5) showed an almost unaltered number of cells in the G₀/G₁-phase (49.4%; 49.5%) and a slight decrease of cells (43.8%) treated with **12**. This observation applies to the ratio of cells in the G₂/M-phase. In G₂/M the cell fraction of the controls showed 15% and 14.9% (WGA/DAPI) whereas cells treated with **12** showed a strong increase of the cell number

(26.1%). S-phase analyses of untreated (35.4%) and WGA/DAPI-control cells (35.3%) revealed no change. The TMZ-probe **12** showed an inverse ratio and a continuous decrease of the cell fraction was detected (29.9%).

Cell membrane structures after 48 h were dispersed to a large extent and hardly detectable. Nevertheless, the blue nuclear (DAPI) and red fluorescent perinuclear structures (Cy7) were still visible indicating the cell killing effect of the theranostic molecule **12** by the TMZ. The cell cycle analysis after 48 h treatment showed the following distribution: untreated controls and the WGA/DAPI-control showed a nearly identical increase of cell number in the G₀/G₁ phase, namely 67.9% and 68.4%. The cells treated with **12**, revealed a strong decrease of cell number in the G₀/G₁-fraction (38.1%). In the G₂/M-phase, cell number ratio of 11.6% and 15.3% in untreated and WGA/DAPI-control cells, respectively, appeared unchanged. The cell fraction in the S-phase accounted for 31.7% after treatment with **12**. The differing S-phase of the untreated control and WGA/DAPI-control cells decreased (20.4%) and (16.1%), respectively. The decreased amount of cells in the G₀/G₁- and in the G₂/M-phase, as well as the increase in the S-phase postulates an arrest of the cell cycle in the S-phase. Additionally, it suggests a post-mitotic cell death after the passage across the G₂/M-phase. Originally, such a process was observed as a consequence of accumulated cell damage caused

by different irradiation effects in radio-sensitivity studies [34-36]. Such a phenomenon was already documented in cell cycle studies with functionalized TMZ on primary TMZ-resistant TP366 glioblastoma cells [24].

The comparison of the cell cycle distribution of all investigated cell lines was time-dependent (24 h, 48 h). A clear increase of the debris fraction was noted in all examined cell lines after treatment with **12**: R3327 cells from 15.8% to 32.6%; DU-145 cells from 19.9% to 43.4%; MDA-MB cells from 25.2% to 41.5%, and Mat_{L_y/Lu} cells from 14% to 27.5%. The amount of debris in the untreated control cells as well as in WGA/DAPI-control cells averaged from 13% to 49% and from 23.1% to 66.4% (R3327); from 11% to 8.9% and 13.7% to 4.4% (DU-145); from 10.6% to 11% and 10.9 to 5.7% (MDA-MB-231) and from 15%, to 8.2% and 12.3 to 23.1% (Mat_{L_y/Lu}) after 24 h and 48 h, respectively (Table 1).

Importantly, the time dependent increase of the number of cells in the S-phase was observed in all cell lines (averaged between 21.1% and 31.7%) except in the DU-145 cells, which showed a decrease from 30.3% to 23% whereas the controls (untreated cells and WGA/DAPI-stained) showed fractions of the S-phase between 7.3% and 6.8%, respectively.

In parallel, a strong decrease of the fraction of the cell lines in the G₂/M-phase treated with **12** for 24 h and 48 h could be assessed: 11.8% and 6.6% (DU-145); 11.4% and 8.2% (MDA-MB-231), respectively. The G₂/M-phase cells fraction of the Mat_{L_y/Lu} cells was constant at 20.7%, 21.5% whereas the R3327 cell fraction increased from 26.1% to 30%. The G₂/M-phase fractions of the controls showed an inconspicuous pattern (Table 1 A-D).

Multiparametric flow cytometry studies

High resolution multiparametric flow cytometry analyses were performed to investigate the damaging processes on R3327 cells, caused by **12** (Figure 3).

We tested two major cell parameters: dot plots representing the cells size and granularity, influenced by the morphology of the cell, the structure of the nuclei and the quantity of cytoplasm-localized compartments (including mitochondria and Golgi) whose count number of intact cells in quadrant analysis QB1 increased over time after the application of **12** from 48.6% (20 min) and 59.4% (24 h) until 71.2% (48 h). Quadrant analysis QB3 assessed cell shrinking, influenced by cell death and/or apoptosis. The cell fraction characterized by clearly increased cell granularity from 54.3% (20 min) to 89.2% (24 h) pointed out strong membrane effects, whereas the subsequent decrease to 28.6% at 48h after the onset of treatment with **12** suggested disintegration processes of mor-

phological membrane structures (Figure 3, column 2).

Discussion

Theranostic conjugate presented here is the prototype of multifunctional adducts based on the 3-mercapto-propionic-cyclohexenyl-Cy7-norbornenyl-bromide-CPP, characterized by a modular structure consisting of units with different functional molecules. CPP is a peptide-based module which harbours a helical structure possessing physico-chemical properties of an amphiphilic behaviour which facilitates the passage of molecules across cellular membranes [37-39]. Its mechanisms of action and the transport efficiency are well documented [40-42]. As a cargo, the Cy7-like molecule is here covalently linked to CPP using the SPPS according to the protocols of Merrifield [4] and Carpino [43]. Of note, we functionalized Cy7-like molecule at the cyclohexene via a thioether with a propionic acid for SPPS chemistry (**9**). The Cy7 can act as a NIR fluorescent dye [14,44].

In order to broaden the application field of Cy7, not restricting it to the imaging purposes, we further functionalized the 2,2,3-trimethyl-3H-indole **2** of the Cy7 at the indolenium nitrogen to the aminopropyl-indolenium-bromide **3** which in turn was reacted to the product norbornenyl-aminopropyl-indolenium-bromide **5** (supplementary information [Figure S2]). The resulting 3-mercapto-propionic acid-cyclohexenyl-Cy7-bis-norbornenyl-bromide **9** possesses functional groups which open a broad spectrum of conjugating properties: (i) the carboxylic group serving as the coupling site for SPPS; (ii) the functionalization with a norbornenyl molecule to the N-indolenium via an aminopropyl group acting as a dienophile reaction partner for *click chemistry* [45] of the classical DAR [1,2] and of the DAR_{inv} [46]; and (iii) the Cy7-like molecule, as described here, not limited to the NIR imaging function but also serving as a spacer in order to avoid sterical interactions between the cargo molecules (imaging components and/or active substances) which may adversely affect the different ligation reaction processes.

We demonstrated here the functionalization of the Cy-based linker by ligation of the pharmacologically active substance TMZ. The combination of chemotherapeutics with different modes of action and of targeting and variability of the number of ligated molecules [47] enables local concentrations sufficient for cell killing of therapy-resistant tumor cells.

Here we employed the multiparameter flow cytometry for a detection of influence of the theranostic conjugate on the cell metabolism, including cell cycle phase, accumulations of cells blocked in particular cell cycle phase, as reviewed by Larsen [48].

Our observations of an increase of the cell debris as well as the decrease of the fraction of the G2/M-phase after treatment with **12** and accumulation of the cells in the S-phase, suggest S-phase blockage followed by a cell death process.

In an analogous manner, the extension of the variant **11** by ligating compounds applicable in additional imaging options (MRI, PET, SPECT and CT) could help in delineating the tumor from the surrounding healthy tissue, a feature that no currently applied imaging modality fulfils exactly.

Development of imaging modalities for diagnostic purposes progressed significantly during the last decade, yet imaging readouts did not reach the accuracy of histological evidences from the patient biopsy material. Although the applicability of MRI for the diagnosis of prostate cancer (PC) advanced substantially, its use in early-stage prostatic cancer, for example, remains very limited, in particular due to the relatively low MRI sensitivity and specificity. Unenhanced MRI is the diagnostic modality of choice since the use of contrast agents (e.g. gadolinium-based) does not improve the diagnostic properties significantly. Therefore, histological verification of the tissue obtained by means of transrectal biopsy remains a golden standard in the prostate cancer diagnosis.

The existence of a selective CA could enable the localization of small, intra-tumour areas of specific characteristics and their treatment. This approach in diagnostic imaging is of interest also for the visualization of invasive properties of the tumor.

Recent molecular imaging studies using MRI alone or in combination with MR spectroscopy (MRI, MRSI, PET) [49] allow a certain optimism that applications of imaging modalities with improved, specific *in-vivo* histology characteristics may be a matter of near future. New approaches to visualize, image and to treat these crucial areas of actively invading tumor have the potential to improve treatment outcome.

Finally, coupling of diagnostic molecules with therapeutic agents (cytostatic, immuno-modulatory or radioactive) and ligation of radio- and chemo-sensitizing molecules may significantly improve chemotherapeutic approaches broadening the spectrum of cancer treatment options.

Supplementary Material

Figures S1- S7.

<http://www.thno.org/v06p0131s1.pdf>

Acknowledgements

This work was supported in part by the *Deutsche Krebshilfe* (project number 106335). Support by the DKFZ Light Microscopy Core Facility is gratefully

acknowledged. The authors are grateful to Renate Bangert, Lisa Seyler, Katja Oehme, and Peter Lorenz for their excellent technical assistance.

DK, MW, WW, VE, RP, HHS, and JD dedicate this work to Klaus Braun who passed away suddenly on 9th August 2015.

Competing interests

The authors have declared that no financial or commercial conflict of interest exists.

References

- [1] Alder K, Diels O. [Otto Diels and Kurt Alder; winners of the Nobel Prize in chemistry.]. *Cienc Invest.* 1951; 7: 143-4.
- [2] Bachmann WE, Chamerda JM. The Diels Alder Reaction of 1-Vinyl-6-Methoxy-3,4-Dihydronaphthalene with Citraconic Anhydride. *J Am Chem Soc.* 1948; 70: 1468-73.
- [3] Merrifield B. Solid-Phase Synthesis. *Science.* 1986; 232: 341-7.
- [4] Merrifield RB. Solid Phase Peptide Synthesis. I The Synthesis of a Tetrapeptide. *J Am Chem Soc.* 1963; 85: 2149-54.
- [5] Merrifield B. Concept and early development of solid-phase peptide synthesis. *Solid-Phase Peptide Synthesis.* 1997; 289: 3-13.
- [6] Muratovska A, Eccles MR. Conjugate for efficient delivery of short interfering RNA (siRNA) into mammalian cells. *Febs Letters.* 2004; 558: 63-8.
- [7] Yoneda F, Suzuki K, Nitta Y. A New Hydrogen-Abstracting Reaction with Diethyl Azodicarboxylate. *J Org Chem.* 1967; 32: 727-9.
- [8] Kosower NS, Kosower EM, Wertheim B, et al. Diamide, A New Reagent for Intracellular Oxidation of Glutathione to Disulfide. *Biochemical and Biophysical Research Communications.* 1969; 37: 593-6.
- [9] Evans BJ, Doi JT, Musker WK. Kinetics of the Aqueous Periodate-Oxidation of Aliphatic Disulfides and Thioethers. *J Org Chem.* 1990; 55: 2580-6.
- [10] Pipkorn R, Waldeck W, Jenne JW, et al. Generation, application and quantification of clamp-BioShuttle carriers for plasmid delivery into nuclei of prostate cancer cells. *Biochem Soc Trans.* 2007; 35: 829-32.
- [11] Weissleder R, Mahmood U. Molecular imaging. *Radiology.* 2001; 219: 316-33.
- [12] Petrovsky A, Schellenberger E, Josephson L, et al. Near-infrared fluorescent imaging of tumor apoptosis. *Cancer Res.* 2003; 63: 1936-42.
- [13] Ernst LA, Gupta RK, Mujumdar RB, et al. Cyanine dye labeling reagents for sulfhydryl groups. *Cytometry.* 1989; 10: 3-10.
- [14] Wiessler M, Hennrich U, Pipkorn R, et al. Theranostic cRGD-BioShuttle Constructs Containing Temozolomide- and Cy7 For NIR-Imaging and Therapy. *Theranostics.* 2011; 1: 381-94.
- [15] Ballou B, Fisher GW, Deng JS, et al. Cyanine fluorochrome-labeled antibodies in vivo: assessment of tumor imaging using Cy3, Cy5, Cy5.5, and Cy7. *Cancer Detect Prev.* 1998; 22: 251-7.
- [16] Wiessler M, Waldeck W, Pipkorn R, et al. The Diels-Alder-Reaction with inverse Electron-Demand - A Review of an efficient & attractive Click-Reaction Concept. *Int J Pharm Sci Res.* 2013; 4: 3678-98.
- [17] Konig K. Multiphoton microscopy in life sciences. *J Microsc.* 2000; 200: 83-104.
- [18] Pansare V, Hejazi S, Faenza W, et al. Review of Long-Wavelength Optical and NIR Imaging Materials: Contrast Agents, Fluorophores and Multifunctional Nano Carriers. *Chem Mater.* 2012; 24: 812-27.
- [19] Spahn G, Felmet G, Baumgarten G, et al. [Evaluation of cartilage degeneration by near infrared spectroscopy (NIRS): methodical description and systematic literature review]. *Z Orthop Unfall.* 2013; 151: 31-7.
- [20] Yu G. Near-infrared diffuse correlation spectroscopy in cancer diagnosis and therapy monitoring. *J Biomed Opt.* 2012; 17: 010901.
- [21] Sevcik-Muraca EM. Translation of near-infrared fluorescence imaging technologies: emerging clinical applications. *Annu Rev Med.* 2012; 63: 217-31.
- [22] Stevens M, Hickman JA, Langdon SP, et al. Antitumor activity and pharmacokinetics in mice of 8-carbamoyl-3-methyl-imidazo[5,1-d]-1,2,3,5-tetrazin-4(3H)-one (CCRG 81045; M & B 39831), a novel drug with potential as an alternative to dacarbazine. *Cancer Res.* 1987; 47: 5846-52.
- [23] Braun K, Wiessler M, Ehemann V, et al. Treatment of glioblastoma multiforme cells with temozolomide-BioShuttle ligated by the inverse Diels-Alder ligation chemistry. *Drug Design, Development and Therapy.* 2008; 2: 289-301.
- [24] Waldeck W, Wiessler M, Ehemann V, et al. TMZ-BioShuttle--a reformulated temozolomide. *Int J Med Sci.* 2008; 5: 273-84.
- [25] Ehemann V, Hashemi B, Lange A, et al. Flow cytometric DNA analysis and chromosomal aberrations in malignant glioblastomas. *Cancer Lett.* 1999; 138: 101-6.
- [26] Boehme WR, Schipper E, Scharpf WG, et al. Stereochemistry of Diels-Alder Adducts .2. the Alkylation of Some Bicyclic Nitriles. *Journal of the American Chemical Society.* 1958; 80: 5488-95.
- [27] Maiti KK, Dinis US, Animesh S, et al. Multiplex targeted in vivo Cancer Detection using sensitive near.infrared SERS nanotags. *Nano Today.* 2012; 7: 85-93.

- [28] Li Q, Tan J, Peng B-X. Synthesis and Characterization of Heptamethine Cyanine Dyes. *Molecules*. 1997; 2: 91-8.
- [29] Reynolds GA, Drexhage KH. Stable Heptamethine Pyrylium Dyes that absorb in the Infrared. *J ORG CHEM*. 1977; 42: 885-8.
- [30] Hilderbrand SA, Kelly KA, Weissleder R, et al. Monofunctional near-infrared fluorochromes for imaging applications. *Bioconjug Chem*. 2005; 16: 1275-81.
- [31] Wiessler M, Kliem C, Lorenz P, Mueller E, and Fleischhacker H. EU Patent: Ligation reaction based on the Diels Alder Reaction with inverse electron demand. [EP 06 012 414.6]. 6-10-2006.
- [32] Pipkorn R, Waldeck W, Diding B, et al. Inverse-electron-demand Diels-Alder reaction as a highly efficient chemoselective ligation procedure: Synthesis and function of a BioShuttle for temozolomide transport into prostate cancer cells. *J Pept Sci*. 2009; 15: 235-41.
- [33] Wiessler M, Waldeck W, Kliem C, et al. The Diels-Alder-reaction with inverse-electron-demand, a very efficient versatile click-reaction concept for proper ligation of variable molecular partners. *Int J Med Sci*. 2009; 7: 19-28.
- [34] Braun K, Wolber G, Waldeck W, et al. The enhancement of neutron irradiation of HeLa-S cervix carcinoma cells by cell-nucleus-addressed deca-p-boronophenylalanine. *Eur J Med Chem*. 2003; 38: 587-95.
- [35] Spunberg JJ, Geard CR, Rutledge-Freeman MH. A comparison of the cytological effects of three hypoxic cell radiosensitizers. *Int J Radiat Oncol Biol Phys*. 1982; 8: 1207-15.
- [36] Varmark H, Sparks CA, Nordberg JJ, et al. DNA damage-induced cell death is enhanced by progression through mitosis. *Cell Cycle*. 2009; 8: 2951-63.
- [37] Derossi D, Chassaing G, Prochiantz A. Trojan peptides: the penetratin system for intracellular delivery. *Tr Cell Biol*. 1998; 8: 84-7.
- [38] Richard JP, Melikov K, Vives E, et al. Cell-penetrating peptides: A re-evaluation of the mechanism of cellular uptake. *J Biol Chem*. 2002; 278: 585-90.
- [39] Braun K, Peschke P, Pipkorn R, et al. A biological transporter for the delivery of peptide nucleic acids (PNAs) to the nuclear compartment of living cells. *J Mol Biol*. 2002; 318: 237-43.
- [40] Richard JP, Melikov K, Vives E, et al. Cell-penetrating peptides. A reevaluation of the mechanism of cellular uptake. *J Biol Chem*. 2003; 278: 585-90.
- [41] Fernandez-Carneado J, Kogan MJ, Pujals S, et al. Amphipathic peptides and drug delivery. *Biopolymers*. 2004; 76: 196-203.
- [42] Persson D, Thoren PE, Lincoln P, et al. Vesicle membrane interactions of penetratin analogues. *Biochemistry*. 2004; 43: 11045-55.
- [43] Carpino LA, Han GY. The 9-Fluorenylmethoxycarbonyl Amino-Protecting Group. *J Org Chem*. 1972; 37: 3404-9.
- [44] Li Z, Sun S, Yang Z, et al. The use of a near-infrared RNA fluorescent probe with a large Stokes shift for imaging living cells assisted by the macrocyclic molecule CB7. *Biomaterials*. 2013; 34: 6473-81.
- [45] Kolb HC, Finn MG, Sharpless KB. Click Chemistry: Diverse Chemical Function from a Few Good Reactions. *Angew Chem Int Ed Engl*. 2001; 40: 2004-21.
- [46] Sauer J, Wiest H. Diels-Alder-Additionen Mit Inversem Elektronenbedarf. *Angew Chem Int Ed Engl*. 1962; 74: 353.
- [47] Wiessler M, Waldeck W, Pipkorn R, et al. Extension of the PNA world by functionalized PNA monomers eligible candidates for inverse Diels Alder Click Chemistry. *Int J Med Sci*. 2010; 7: 213-23.
- [48] Larsen JK. Cell proliferation: analysis by flow cytometry. *Nouv Rev Fr Hematol*. 1992; 34: 317-35.
- [49] Roach M3, Kurhanewicz J, Carroll P. Spectroscopy in prostate cancer: hope or hype? *Oncology (Huntingt)*. 2001; 15: 1399-410.
- [50] Saracoglu N. Recent advances and applications in 1,2,4,5-tetrazine chemistry. *TETRAHEDRON*. 2007; 63: 4199-236.
- [51] Hansell CF, Espeel P, Stamenovic MM, et al. Additive-free clicking for polymer functionalization and coupling by tetrazine-norbornene chemistry. *J Am Chem Soc*. 2011; 133: 13828-31.